1   **Delta spike P681R mutation enhances SARS-CoV-2 fitness over Alpha variant**

2   Yang Liu[1,2,*], Jianying Liu[2,3,4,*], Bryan A. Johnson[4], Hongjie Xia[1], Zhiqiang Ku[5], Craig
3   Schindewolf[2,3,4], Steven G. Widen[1], Zhiqiang An[5], Scott C. Weaver[2,3,4], Vineet D. Menachery[2,3,4],
4   Xuping Xie[1#], and Pei-Yong Shi[1,2,3,#]

5

6   [1]Department of Biochemistry and Molecular Biology, University of Texas Medical Branch,
7   Galveston TX, USA

8   [2]Institute for Human Infections and Immunity, University of Texas Medical Branch, Galveston
9   TX, USA

10   [3]World Reference Center for Emerging Viruses and Arboviruses, University of Texas Medical
11   Branch, Galveston TX, USA

12   [4]Department of Microbiology and Immunology, University of Texas Medical Branch, Galveston
13   TX, USA

14   [5]Texas Therapeutics Institute, Brown Foundation Institute of Molecular Medicine, The University
15   of Texas Health Science Center at Houston, Houston, TX 77030, USA

16

17   *YL and JL made equal contributions to the study

18

19   [#]Correspondence: X.X. (xuxie@UTMB.edu) or P.-Y.S. (peshi@UTMB.edu)

20

21   **Abstract**

22   SARS-CoV-2 Delta variant has rapidly replaced the Alpha variant around the world. The

23   mechanism that drives this global replacement has not been defined. Here we report that Delta

24   spike mutation P681R plays a key role in the Alpha-to-Delta variant replacement. In a replication

25   competition assay, Delta SARS-CoV-2 efficiently outcompeted the Alpha variant in human lung

26   epithelial cells and primary human airway tissues. Delta SARS-CoV-2 bearing the Alpha-spike

27   glycoprotein replicated less efficiently than the wild-type Delta variant, suggesting the

28   importance of Delta spike in enhancing viral replication. The Delta spike has accumulated

29   mutation P681R located at a furin cleavage site that separates the spike 1 (S1) and S2

30   subunits. Reverting the P681R mutation to wild-type P681 significantly reduced the replication

31   of Delta variant, to a level lower than the Alpha variant. Mechanistically, the Delta P681R

32   mutation enhanced the cleavage of the full-length spike to S1 and S2, leading to increased

33   infection via cell surface entry. In contrast, the Alpha spike also has a mutation at the same

34   amino acid (P681H), but the spike cleavage from purified Alpha virions was reduced compared

35   to the Delta spike. Collectively, our results indicate P681R as a key mutation in enhancing Delta

36   variant replication via increased S1/S2 cleavage. Spike mutations that potentially affect furin

37   cleavage efficiency must be closely monitored for future variant surveillance.

38

Introduction

40   The continuous emergence of new variants of severe acute respiratory syndrome

41   coronavirus 2 (SARS-CoV-2) poses the greatest threat to pandemic control, vaccine

42   effectiveness, therapeutic efficacy, and surveillance. Since its emergence in late 2019,

43   mutations have unceasingly emerged in the circulating viruses, leading to variants with

44   enhanced transmissibility, evasion of therapeutic antibodies, and breakthrough infections in

45   vaccinated individuals.[1-6] Since the viral spike glycoprotein is responsible for binding to the

46   human cellular receptor angiotensin-converting enzyme (ACE2), many mutations have

47   accumulated in the spike gene with the potential to alter viral fitness or to escape immunity. The

48   variants have emerged from different geographic regions and, depending on their biological

49   properties, spread to other regions. The World Health Organization (WHO) has classified

50   variants as "variants of concern" (*i.e.*, Alpha, Beta, Gamma, and Delta) and "variants of interest"

51   (*i.e.*, Eta, Iota, Kappa, and Lambda).[7] The Alpha variant was first identified in the United

52   Kingdom in September 2020 and subsequently became dominant in many parts of the world.

53   Afterwards, the Delta variant emerged in India in October 2020 and has now spread to over 119

54   countries, displacing the Alpha variant globally.[7,8] From May 2 to July 31 of 2021, the

55   prevalence of the Delta variant in the USA had increased from 1.3% to 94.4%, whereas the

56   prevalence of the Alpha variant had decreased from 70% to 2.4%. More seriously, the Delta

57   variant has been associated with increased transmissibility, disease severity, and breakthrough

58   infections in vaccinated individuals.[5,9-11] The mutation(s) that have driven the explosive spread

59   of the Delta variant and its displacement of the Alpha variant remain to be defined. In this study,

60   we used a reverse genetic approach to identify the molecular determinant(s) for the enhanced

61   fitness of Delta variant and its dominance over the Alpha variant.

62

63   **Results**

64   We constructed infectious cDNA clones for the Alpha (GISAIS ID: EPI_ISL_999340) and

65   Delta (GISAIS ID: EPI_ISL_2100646) SARS-CoV-2 variants using a previously established

66   protocol (**Extended data Fig. 1**).[12,13] The infectious cDNA clones enabled us to prepare

67   recombinant Alpha and Delta SARS-CoV-2 variants (**Fig. 1a**). Both Alpha and Delta variants

68   rescued from these clones developed smaller plaques on Vero E6 cells than the earlier

69   USA/WA1-2020 (wild-type) strain isolated in January 2020 (**Extended data Fig. 2**). Sequencing

70   analysis showed no undesired mutations in the rescued recombinant virus stocks. To compare

71   the viral replication fitness between the Alpha and Delta variants, we performed a competition

72   assay by infecting cells with a mixture of the two viruses at a plaque-forming unit (PFU) ratio of

73   1:1, followed by quantifying the ratios of the two viral RNA species at different days post

74   infection. Compared with analyzing individual viruses separately, the competition assay has the

75   advantages of (i) a built-in internal control of each viral replication and (ii) elimination of host-to-

76   host variation that reduces experimental power. Due to its precision and reproducibility[14], the

77   competition assay has been widely used to study microbial fitness,[15-17] including SARS-CoV-

78   2[1,18]. When infecting human lung adenocarcinoma Calu-3 cells, the RNA ratio of Delta versus

79   Alpha increased to 3.0, 7.0, and 4.1 at 24, 36, and 48 h post infection, respectively (**Extended**

80   **data Fig. 3**). When infecting primary human airway epithelial (HAE) cultures, the RNA ratio of

3

81   Delta versus Alpha increased from 1.7 on day 1 to 3.1 on day 5 (**Fig. 1b**). These results indicate

82   that Delta variant has greater replication fitness compared to the Alpha variant in *in vitro*

83   respiratory models of SARS-CoV-2 infection.

84   To examine if the spike gene alone determines the improved replication fitness of the

85   Delta variant, we constructed a chimeric Delta SARS-CoV-2 bearing the Alpha-spike

86   glycoprotein (*i.e.*, Alpha-spike/Delta-backbone virus; **Fig. 1a** and **Extended data Fig. 2b**). In a

87   competition assay on HAE culture, the RNA ratio of Delta versus Alpha-spike/Delta-backbone

88   continuously increased from 2.8 on day 1 to 9.8 on day 5 post infection (**Fig. 1c**), suggesting

89   that (i) the Alpha-spike reduces the replication fitness of the Delta variant and (ii) the spike gene

90   drives the improved replication of Delta variant. Interestingly, the Alpha-spike/Delta-backbone

91   virus replicated less efficiently than the Alpha variant on HAE culture (**Fig. 1d**), suggesting that,

92   in contrast to Delta spike mutations that enhance replication, mutations outside the spike gene

93   of the Delta variant reduced to some degree fitness for viral replication. The above

94   quantifications of viral competition outcomes were measured by Sanger sequencing (**Fig. 1b-d**)

95   and subsequently verified by Illumina next generation sequencing (NGS; **Extended data Fig.**

96   **4**).

97   Delta spike has accumulated mutations T19R, G142D, E156G, F157-R158 deletion,

98   L452R, T478K, D614G, P681R, and D950N,[19] among which P681R is located at a furin

99   cleavage site (PRRAR↓S with P681 underlined and "↓" indicating furin cleavage) that is absent

100   in other group 2B coronaviruses.[20] Since the furin cleavage site was shown to be important for

101   SARS-CoV-2 replication and pathogenesis,[21,22] we hypothesized that mutation P681R may

102   improve the furin cleavage efficiency of full-length spike to S1 and S2, leading to a more

103   efficient virus entry into respiratory epithelial cells. To test this hypothesis, we reverted the Delta

104   P681R mutation to wild-type P681 in the Delta SARS-CoV-2 (**Extended data Fig. 2a**). The

105   Delta-P681 virus developed equivalent plaque morphology compared with Delta (**Extended**

4

106   **data Fig. 2b**). Remarkably, the P681 reversion attenuated Delta variant replication on HAE

107   cultures, as evidenced by the increase in the RNA ratio of wild-type Delta versus Delta-P681

108   from 2.2 on day 1 to 3.4 on day 5 (**Fig. 1e**). The replication of the Delta-P681 virus was even

109   lower than that of the Alpha variant, as suggested by the decrease in the RNA ratio of Delta-

110   P681 versus Alpha variant from 0.9 on day 1 to 0.6 on day 5 (**Fig. 1f**). These results

111   demonstrate that mutation P681R at the furin cleavage site plays a critical role in enhancing the

112   replication of the Delta variant on primary human airway cultures.

113   We directly evaluated the spike cleavage of Alpha, Delta, Delta-P681, and wild-type

114   SARS-CoV-2. Virions were prepared from Vero E6 cells expressing TMPRSS2, a host serine

115   protease that is required for SARS-CoV-2 entry via the ACE2-mediated cell surface

116   mechanism.[23] After virions were purified through sucrose cushion ultracentrifugation, pelleted

117   viruses were analyzed for spike cleavage by Western blotting (**Fig. 1g**). The results showed that

118   spike processing efficiency of the purified virions occurred in the order of Delta > Alpha > Delta-

119   P681 > wild-type virions, with ratios of S1 versus full-length spike of 15.3, 5.4, 2.7, and 1.4,

120   respectively (**Fig. 1h**). It should be noted that the Alpha variant also has a spike mutation at

121   amino acid position 681 (P681H), which may contribute to the increase in spike cleavage when

122   compared with the wild-type USA/WA1-2020 virus; however, a recent study showed that

123   mutation P681H alone did not enhance viral fitness or transmission.[4] Overall, our results

124   indicate a correlation of improved spike cleavage with enhanced viral replication of Delta

125   variant.

126   To exclude the possibility that enhanced replication of the Delta variant over Alpha was

127   due to an improved spike/ACE2 receptor interaction, we performed a binding assay using

128   recombinant spike receptor-binding domain (RBD) and human ACE2 proteins on a Bio-Layer

129   Interferometry (BLI) system (**Extended data Fig. 5**). Within the RBD, the Alpha RBD has a

130   N501Y mutation, whereas Delta RBD has L452R and T478K mutations. The BLI results indicate

131   that the Alpha RBD has a higher binding affinity for ACE2 than Delta RBD, as indicated by

132   >200-fold K_D improvement (**Extended data Fig. 5**). These data strongly argue that the higher

133   replication of Delta variant than Alpha variant is not due to an improved spike/ACE2 receptor

134   binding.

135

136   **Discussion**

137   Since the emergence of SARS-CoV-2, the virus has accumulated mutations improving

138   fitness and transmission. First, it accumulated a D614G mutation in the spike gene to enhance

139   viral transmission.[1,3,6,24] This mutation promotes spike RBD in an "open" conformation to

140   facilitate ACE2 receptor binding.[25] Subsequently, another spike mutation N501Y emerged

141   independently in Alpha, Beta, and Gamma variants from the United Kingdom, South Africa, and

142   Brazil, respectively. The N501Y mutation further increases the binding affinity between the spike

143   protein and ACE2, leading to additional improvement in viral transmission.[4,10,26] Most recently,

144   the Delta variant emerged and spread explosively, replacing the Alpha variant around the world.

145   The current study demonstrates that spike mutation(s) are responsible for the enhanced viral

146   fitness of the Delta variant over Alpha. Importantly, the unique P681R mutation plays a critical

147   role in this fitness advantage and increases the processing of Delta spike to S1 and S2, most

148   likely through an improved furin cleavage when newly assembled virions egress through the

149   trans-Golgi network. Although the original SARS-CoV-2 strain has a functional furin cleavage

150   site with a minimal recognition site of RXXR↓,[27] adjacent residues influence the cleavage

151   efficiency.[28] The P681R substitution clearly augments spike processing and is likely the main

152   driver of the fitness advantage observed in Delta variant. When the Delta variant infects

153   respiratory epithelial cells, it binds to ACE2 receptor via the RBD in S1. Already cleaved at the

154   S1/S2 site, the Delta virion facilitates cleavage at S2' by the cell surface protease TMPRSS2,

155   leading to an activation of the S2 fusion peptide (FP) for viral and plasma membrane fusion.[23]

6

156   Thus, the improved spike cleavage enhances viral replication when the Delta variant infects

157   respiratory epithelial cells.

158   One major concern with the emergence of Delta variant is its association with increased

159   breakthrough infections in vaccinated people.[5,9] As a critical target for host immunity, changes in

160   the spike protein of SARS-CoV-2 variants have been implicated in reducing antibody

161   neutralization.[29] Among all tested variants (including Delta), the Beta and Kappa variants have

162   been shown to reduce the BNT162b2 vaccine-elicited neutralizing titers the most;[2,30-32] yet,

163   BNT162b2 showed 100% vaccine efficacy against Beta variant-associated severe, critical or

164   fatal disease in Qatar and 100% real-world effectiveness against Beta variant-associated

165   COVID-19 in South Africa.[33,34] These real-world vaccine efficacy/effectiveness and *in vitro*

166   neutralization results argue that breakthrough infections by the Delta variant in vaccinated

167   individuals do not reflect immune escape. Instead, the increased breakthrough infection is likely

168   due to enhanced viral replication fitness of the Delta variant through augmented spike

169   processing. Consistent with this hypothesis, the viral RNA loads in the oropharynx from Delta

170   variant-infected patients were >1,200-fold higher than those from the original Wuhan virus-

171   infected patients.[9] Together, the results indicate changes in viral processing and infection

172   efficiency, rather than evasion of antibodies, drive breakthrough infections of Delta variant in

173   vaccinated individuals.

174   In summary, using a reverse genetic system and primary human airway cultures, we

175   have identified spike mutation P681R as a significant determinant for enhanced viral replication

176   fitness of the Delta compared to the Alpha variant. The P681R mutation enhances spike protein

177   processing through the improved furin cleavage site. As new variants continue to emerge, spike

178   mutations that affect furin cleavage efficiency, as well as other mutations that may increase viral

179   replication, pathogenesis, and/or immune escape, must be closely monitored.

180

Methods

Cells. African green monkey kidney epithelial Vero E6 cells (ATCC, Manassas, VA, USA) were grown in Dulbecco's modified Eagle's medium (DMEM; Gibco/Thermo Fisher, Waltham, MA, USA) with 10% fetal bovine serum (FBS; HyClone Laboratories, South Logan, UT) and 1% penicillin/streptomycin (Gibco). Human lung adenocarcinoma epithelial Calu-3 cells (ATCC) were maintained in a high-glucose DMEM containing sodium pyruvate and GlutaMAX (Gibco) with 10% FBS and 1% penicillin/streptomycin at 37°C with 5% CO_2. The EpiAirway system is a primary human airway 3D tissue model purchased from MatTek Life Science (Ashland, MA, USA). This EpiAirway system was maintained with the provided culture medium at 37°C with 5% CO_2 following manufacturer's instruction. All other culture medium and supplements were purchased from Thermo Fisher Scientific (Waltham, MA, USA). All cell lines were verified and tested negative for mycoplasma.

Construction of infectious cDNA clones and SARS-CoV-2 mutant viruses. The full-length (FL) cDNA clones of Alpha and Delta variants were constructed through mutagenesis of a previously established cDNA clone of USA/WA1-2020 SARS-CoV-2.[12,13] The previous seven-fragment *in vitro* ligation method was improved to a three-fragment ligation approach (**Extended data Fig. 1a**) to construct the full-length cDNA clones of Alpha and Delta SARS-CoV-2, resulting in Alpha-FL and Delta-FL, respectively. Prior to the three-fragment ligation, mutations from Alpha or Delta variants were engineered into individual fragments of USA/WA1-2020 using a standard mutagenesis method. The sequences for constructing Alpha, Delta and Alpha-spike/Delta-backbone were downloaded from GISAID database, the accession ID for Alpha is EPI_ISL_999340, accession ID for Delta is EPI_ISL_2100646. Individual point mutations for Alpha (NSP3: P153L, T183I, A890D, I1412T; NSP6: SGF106-108del; NSP12: P323L; Spike: HV69-70del, Y145del, N501Y, A570D, D614G, P681H, T716I, S982A, D1118H; ORF8: Q27stop, R52I, Y73C, S84L; N: D3L, R203K, G204R, S235F) and individual point mutations for

8

206   Delta (NSP2: P129L; NSP3: P822L; H1274Y; NSP4: A446V; NSP6: V149A; NSP12: P323L;

207   V355A; G671S; NSP13: P77L; NSP15: H234Y; Spike: T19R, G142D, E156G, FR157-158del,

208   L452R, T478K, D614G, P681R, D950N; ORF3a: S26L; M: I82T; ORF7a: V82A; L116F; T120I;

209   ORF8: S84L; DF119-120del; N: D63G; R203M; D377Y; R385K) were introduced into subclones

210   of individual fragments by overlapping fusion PCR. For preparing Alpha-spike/Delta-backbone

211   virus, the spike gene of Delta was replaced with the spike gene of the Alpha. For preparing

212   Delta-P681 virus, the P681 reversion was introduced into a subclone containing Delta spike

213   gene by overlapping fusion PCR. All primers used for the construction were listed in **Extended**

214   **Data Table 1**. The full-length infectious clones of SARS-CoV-2 variants were assembled by *in*

215   *vitro* ligation of contiguous DNA fragments. *In vitro* transcription was then performed to

216   synthesize full-length genomic RNA. For recovering recombinant viruses, the RNA transcripts

217   were electroporated into Vero E6 cells. The viruses from electroporated cells were harvested at

218   40 h post electroporation and served as P0 stocks. All viruses were passaged once on Vero E6

219   cells to produce P1 stocks for subsequent experiments. All P1 viruses were subjected to next

220   generation sequencing to confirm the introduced mutations without undesired changes. Viral

221   titers were determined by plaque assay on Vero E6 cells. All virus preparation and experiments

222   were performed in a biosafety level 3 (BSL-3) facility. Viruses and plasmids are available from

223   the World Reference Center for Emerging Viruses and Arboviruses (WRCEVA) at the University

224   of Texas Medical Branch.

225   **RNA extraction, RT-PCR, and Sanger sequencing.** Cell culture supernatants were

226   mixed with a five-fold excess of TRIzol™ LS Reagent (Thermo Fisher Scientific, Waltham, MA,

227   USA). Viral RNAs were extracted according to the manufacturer's instructions. The RNAs were

228   amplified using a SuperScript™ III One-Step RT-PCR kit (Invitrogen, Carlsbad, CA, USA)

229   following the manufacturer's protocol. The size of desired amplicon was verified with 2 µl of

230   PCR product on an agarose gel. The remaining 18 µl of RT-PCR DNA was purified by a

231 QIAquick PCR Purification kit (Qiagen, Germantown, MD, USA). Sequences of the purified RT-

232 PCR products were generated using a BigDye Terminator v3.1 cycle sequencing kit (Applied

233 Biosystems, Austin, TX, USA). The sequencing reactions were purified using a 96-well plate

234 format (EdgeBio, San Jose, CA, USA) and analyzed on a 3500 Genetic Analyzer (Applied

235 Biosystems, Foster City, CA). The peak electropherogram height representing each mutation

236 site and the proportion of each competitor was analyzed using the QSVanalyser program. For

237 the competition assay, R software is used for the figure generation and statistical analysis. The

238 presented viral RNA ratios in the figures were normalized by the input viral RNA ratios

239 (**Extended Data Table 2**).

240   **Plaque assay.** Approximately 1.2×10^6 Vero E6 cells were seeded to each well of 6-well

241 plates and cultured at 37°C, 5% CO_2 for 16 h. Virus was serially diluted in DMEM with 2% FBS

242 and 200 µl diluted viruses were transferred onto the cell monolayers. The viruses were

243 incubated with the cells at 37°C with 5% CO_2 for 1 h. After the incubation, overlay medium was

244 added to the infected cells per well. The overlay medium contained DMEM with 2% FBS, 1%

245 penicillin/streptomycin, and 1% sea-plaque agarose (Lonza, Walkersville, MD). After 2.5-day

246 incubation, plates were stained with neutral red (Sigma-Aldrich, St. Louis, MO, USA) and

247 plaques were counted on a light box.

248   **Next generation sequencing (NGS).** The competition results generated by Sanger

249 sequencing were confirmed using NGS methods. Briefly, viral RNA samples from competition

250 groups of (i) Delta versus Alpha and (ii) Delta versus Alpha-spike/Delta-backbone were used for

251 a specific one-step RT-PCR that containing the A23063T mutation site. Viral RNA samples from

252 competition group of Alpha versus Alpha-spike/Delta-backbone were quantified by the T14444C

253 mutation. The RT-PCR primers were listed in **Extended Data Table 1**. The PCR products were

254 purified by a QIAquick PCR Purification kit (Qiagen, Germantown, MD) according to the

255 manufacturer's protocol. Dual-indexed adapter sequences (New England BioLabs, Ipswich, MA)

10

256   were added with 5 cycles of PCR. Samples were pooled and sequenced on an Illumina MiniSeq

257   Mid-Output flow cell with the paired-end 150 base protocol. The reads were filtered for Q-scores

258   of 37 at the A23063T and T14444C mutation sites and adjacent bases and counted. For the

259   competition assay, R software is used for the figure generation and statistical analysis.

260   **Viral infection of cell lines.** Approximately 3×10^5 Calu-3 cells were seeded onto each

261   well of 12-well plates and cultured at 37°C, 5% CO_2 for 16 h. Equal PFUs of two viruses were

262   inoculated onto Calu-3 cells at a final MOI of 0.1. The mixed viruses were incubated with the

263   cells at 37°C for 2 h. After infection, the cells were washed thrice with DPBS to remove residual

264   viruses. One milliliter of culture medium was added into each well. At each time point, 100 µl of

265   culture supernatants were lysed in TRIzol LS reagent for the detection of competition assay,

266   and 100 µl of fresh medium was added into each well to replenish the culture volume. The cells

267   were infected in triplicate for each group of viruses. All samples were stored at -80°C until

268   analysis.

269   **Primary human airway cultures.** The EpiAirway system is a primary human airway 3D

270   mucociliary tissue model consisting of normal, human-derived tracheal/bronchial epithelial cells.

271   Different combinations of mixed viruses for competition assays were inoculated onto the culture

272   at a total MOI of 5. After 2 h infection at 37 °C with 5% CO_2, the inoculum was removed, and the

273   culture was washed three times with DPBS. The infected epithelial cells were maintained

274   without any medium in the apical well, and medium was provided to the culture through the

275   basal well. The infected cells were incubated at 37 °C, 5% CO_2. From day 1 to day 5 post

276   infection, 300 µl of DPBS were added onto the apical side of the airway culture and incubated at

277   37°C for 30 min to elute progeny viruses. All virus samples in DPBS were stored at –80°C and

278   quantified by plaque assays on Vero E6 cells.

279   **Virion purification and Western blotting.** Vero E6 expressing TMPRSS2 were

280   infected with different SARS-CoV-2 at an MOI of 0.01. At 24 h post infection, the culture

281 medium was collected, purified through a 20% sucrose cushion, and analyzed by Western blot

282 as previously described.[21] Densitometry was performed to quantify the cleavage efficiency of

283 full-length spike to S1/S2 subunits using ImageLab 6.0.1 (Bio-Rad #12012931). The average

284 results of two experiments were presented.

285 **Spike RBD and ACE2 binding.** The human ACE2 protein was purchased from Sino

286 Biological (Beijing, China; Cat# 10108-H08H) and the human IgG1 Fc-tagged RBD proteins

287 were made in-house using a method as previously described[35]. The affinity measurement was

288 performed on the ForteBio Octet RED 96 system (Sartorius, Goettingen, Germany). Briefly, the

289 RBD proteins (20 µg/ml) of Alpha or Delta RBDs were captured onto protein A biosensors for

290 300s. The loaded biosensors were then dipped into the kinetics buffer for 10 s for adjustment of

291 baselines. Subsequently, the biosensors were dipped into serially diluted (from 1.23 to 300 nM)

292 human ACE2 protein for 200 s to record association kinetics and then dipped into kinetics buffer

293 for 400 s to record dissociation kinetics. Kinetic buffer without ACE2 was used to correct the

294 background. The Octet Data Acquisition 9.0 software was used to collect affinity data. For fitting

295 of K_D values, Octet Data Analysis software V11.1 was used to fit the curve by a 1:1 binding

296 model using the global fitting method.

297 **Statistics.** For virus competition experiments, relative replicative fitness values for

298 different variants were analyzed according to w=(f0/i0), where i0 is the initial two-virus ratio and

299 f0 is the final two-virus ratio after competition. Sanger sequencing (initial timepoint T0) counts

300 for each virus being compared were based upon average counts over three replicate samples of

301 inocula per experiment, and post-infection (timepoint T1) counts were taken from samples of

302 individual subjects. Multiple experiments were performed, so that f0/i0 was clustered by

303 experiment. To model f0/i0, the ratio T0/T1 was found separately for each subject in each virus

304 group, log (base-10) transformed to an improved approximation of normality and modeled by

305 analysis of variance with relation to group, adjusting by experiment when appropriate to control

306   for   clustering   within   experiment.   Specifically,   the   model   was   of   the   form

307   Log10_CountT1overCountT0 ~ Experiment + Group. Fitness ratios between the two groups [the

308   model's estimate of w=(f0/i0)] were assessed per the coefficient of the model's Group term,

309   which was transformed to the original scale as 10^coefficient. This modeling approach

310   compensates for any correlation due to clustering within experiment similarly to that of

311   corresponding mixed effect models and is effective since the number of experiments was small.

312   Statistical analyses were performed using R statistical software (R Core Team, 2019, version

313   3.6.1). In all statistical tests, two-sided alpha=.05. Catseye plots[36], which illustrate the normal

314   distribution of the model-adjusted means, were produced using the "catseyes" package[37].

315

Data availability.

317   Extended Data and source data for generating main figures are available in the online

318   version of the paper. Any other information is available upon request.

319

Acknowledgments

329

Author contributions

331   Conceptualization, Y.L., J.L., S.C.W., V.D.M., X.X., P.-Y.S.; Methodology, Y.L., J.L.,

332 B.A.J., H.X., Z.K., C.S., S.G.W., Z.A., X.X.; Investigation, Y.L., J.L., B.A.J., H.X., Z.A., S.C.W.,

333 V.D.M., X.X., P.-Y.S.; Resources, H.X., B.A.J., Z.K., Z.A. X.X.; Data Curation, Y.L., J.L., B.A.J.,

334 H.X., Z.K., C.S., S.C.W., V.D.M., X.X., P.-Y.S.; Writing-Original Draft, Y.L., J.L, X.X., P.-Y.S;

335 Writing-Review & Editing, Y.L., J.L., B.A.J., H.X., Z.K., C.S., S.G.W., Z.A., S.C.W., V.D.M., X.X.,

336 P.-Y.S.; Supervision, X.X., S.C.W., V.D.M., P.-Y.S.; Funding Acquisition, Z.A., S.C.W., V.D.M.,

337 P.-Y.S.

338

Competing financial interests

340   X.X., V.D.M., and P.-Y.S. have filed a patent on the reverse genetic system and reporter

341 SARS-CoV-2. Other authors declare no competing interests.

342

References

344 1   Plante, J. A. *et al.* Spike mutation D614G alters SARS-CoV-2 fitness. *Nature* **592**, 116-121,
345   doi:10.1038/s41586-020-2895-3 (2021).
346 2   Chen, R. E. *et al.* Resistance of SARS-CoV-2 variants to neutralization by monoclonal and serum-
347   derived polyclonal antibodies. *Nat Med* **27**, 717-726, doi:10.1038/s41591-021-01294-w (2021).
348 3   Hou, Y. J. *et al.* SARS-CoV-2 D614G variant exhibits efficient replication ex vivo and transmission
349   in vivo. *Science* **370**, 1464-1468, doi:10.1126/science.abe8499 (2020).
350 4   Liu, Y. *et al.* The N501Y spike substitution enhances SARS-CoV-2 transmission. *bioRxiv*,
351   doi:10.1101/2021.03.08.434499 (2021).
352 5   Brown, C. M. *et al.* Outbreak of SARS-CoV-2 Infections, Including COVID-19 Vaccine
353   Breakthrough Infections, Associated with Large Public Gatherings — Barnstable County,
354   Massachusetts, July 2021. *Morbidity and Mortality Weekly Report (MMWR)*,
355   https://www.cdc.gov/mmwr/volumes/70/wr/mm7031e7032.htm?s_cid=mm7031e7032_w&fbc
356   lid=IwAR7032WV7036ul_A-l_VN_7015KX7034bedb7038CeLJKRwiDWZ-
357   bIUuWmZMKbs7094xdhTiPLs (2021).

358 6   Zhou, B. *et al.* SARS-CoV-2 spike D614G change enhances replication and transmission. *Nature*
359   **592**, 122-127, doi:10.1038/s41586-021-03361-1 (2021).
360 7   WHO. Track SARS-CoV-2 variants. https://www.who.int/en/activities/tracking-SARS-CoV-2-
361   variants/ (2021).
362 8   CDC. COVID data tracker. https://covid.cdc.gov/covid-data-tracker/#variant-proportions (2021).
363 9   Li, B. *et al.* Viral infection and transmission in a large, well-traced outbreak caused by the SARS-
364   CoV-2 Delta variant. *medRxiv*,
365   https://www.medrxiv.org/content/10.1101/2021.1107.1107.21260122v21260122 (2021).
366 10   Mlcochova, P. *et al.* SARS-CoV-2 B.1.617.2 Delta variant emergence, replication and sensitivity to
367   neutralising antibodies. *BioRxiv* (2021).
368 11   Chia, P. Y. *et al.* Virological and serological kinetics of SARS-CoV-2 Delta variant vaccine2
369   breakthrough infections: a multi-center cohort study. *medRxiv*,
370   https://www.medrxiv.org/content/10.1101/2021.1107.1128.21261295v21261291 (2021).
371 12   Xie, X. *et al.* An Infectious cDNA Clone of SARS-CoV-2. *Cell Host Microbe* **27**, 841-848 e843,
372   doi:10.1016/j.chom.2020.04.004 (2020).
373 13   Xie, X. *et al.* Engineering SARS-CoV-2 using a reverse genetic system. *Nature Protocols* **16**, 1761-
374   1784, doi:10.1038/s41596-021-00491-8 (2021).
375 14   Liu, J. *et al.* Role of mutational reversions and fitness restoration in Zika virus spread to the
376   Americas. *Nat Commun* **12**, 595, doi:10.1038/s41467-020-20747-3 (2021).
377 15   Wiser, M. J. & Lenski, R. E. A Comparison of Methods to Measure Fitness in Escherichia coli. *PLoS*
378   *One* **10**, e0126210, doi:10.1371/journal.pone.0126210 (2015).
379 16   Grubaugh, N. D. *et al.* Genetic Drift during Systemic Arbovirus Infection of Mosquito Vectors
380   Leads to Decreased Relative Fitness during Host Switching. *Cell Host Microbe* **19**, 481-492,
381   doi:10.1016/j.chom.2016.03.002 (2016).
382 17   Bergren, N. A. *et al.* "Submergence" of Western equine encephalitis virus: Evidence of positive
383   selection argues against genetic drift and fitness reductions. *PLoS Pathog* **16**, e1008102,
384   doi:10.1371/journal.ppat.1008102 (2020).
385 18   Touret, F. *et al.* Replicative Fitness of a SARS-CoV-2 20I/501Y.V1 Variant from Lineage B.1.1.7 in
386   Human Reconstituted Bronchial Epithelium. *mBio*, e0085021, doi:10.1128/mBio.00850-21
387   (2021).
388 19   Organization, W. H. Coronavirus Disease (COVID-19): Weekly Epidemiological Update.
389   *https://reliefweb.int/report/world/coronavirus-disease-covid-19-weekly-epidemiological-*
390   *update-11-may-2021* (2021).
391 20   Coutard, B. *et al.* The spike glycoprotein of the new coronavirus 2019-nCoV contains a furin-like
392   cleavage site absent in CoV of the same clade. *Antiviral Res* **176**, 104742,
393   doi:10.1016/j.antiviral.2020.104742 (2020).
394 21   Johnson, B. A. *et al.* Loss of furin cleavage site attenuates SARS-CoV-2 pathogenesis. *Nature* **591**,
395   293-299, doi:10.1038/s41586-021-03237-4 (2021).
396 22   Peacock, T. P. *et al.* The furin cleavage site in the SARS-CoV-2 spike protein is required for
397   transmission in ferrets. *Nat Microbiol* **6**, 899-909, doi:10.1038/s41564-021-00908-w (2021).
398 23   Murgolo, N. *et al.* SARS-CoV-2 tropism, entry, replication, and propagation: Considerations for
399   drug discovery and development. *PLoS Pathog* **17**, e1009225, doi:10.1371/journal.ppat.1009225
400   (2021).
401 24   Korber, B. *et al.* Tracking Changes in SARS-CoV-2 Spike: Evidence that D614G Increases
402   Infectivity of the COVID-19 Virus. *Cell* **182**, 812-827 e819, doi:10.1016/j.cell.2020.06.043 (2020).
403 25   Yurkovetskiy, L. *et al.* Structural and Functional Analysis of the D614G SARS-CoV-2 Spike Protein
404   Variant. *Cell* **183**, 739-751, doi:10.1016/j.cell.2020.09.032 (2020).

405   26   Wan, Y., Shang, J., Graham, R., Baric, R. S. & Li, F. Receptor Recognition by the Novel Coronavirus
406   from Wuhan: an Analysis Based on Decade-Long Structural Studies of SARS Coronavirus. *J Virol*
407   **94**, doi:10.1128/JVI.00127-20 (2020).
408   27   Molloy, S. S., Bresnahan, P. A., Leppla, S. H., Klimpel, K. R. & Thomas, G. Human furin is a
409   calcium-dependent serine endoprotease that recognizes the sequence Arg-X-X-Arg and
410   efficiently cleaves anthrax toxin protective antigen. *Journal of Biological Chemistry* **267**, 16396-
411   16402 (1992).
412   28   Krysan, D. J., Rockwell, N. C. & Fuller, R. S. Quantitative characterization of furin specificity.
413   Energetics of substrate discrimination using an internally consistent set of hexapeptidyl
414   methylcoumarinamides. *J Biol Chem* **274**, 23229-23234, doi:10.1074/jbc.274.33.23229 (1999).
415   29   Plante, J. A. *et al.* The variant gambit: COVID-19's next move. *Cell Host Microbe* **29**, 508-515,
416   doi:10.1016/j.chom.2021.02.020 (2021).
417   30   Liu, Y. *et al.* Neutralizing Activity of BNT162b2-Elicited Serum. *N Engl J Med* **384**, 1466-1468,
418   doi:10.1056/NEJMc2102017 (2021).
419   31   Liu, Y. *et al.* BNT162b2-Elicited Neutralization against New SARS-CoV-2 Spike Variants. *N Engl J*
420   *Med*, doi:10.1056/NEJMc2106083 (2021).
421   32   Liu, J. *et al.* BNT162b2-elicited neutralization of B.1.617 and other SARS-CoV-2 variants. *Nature*,
422   doi:10.1038/s41586-021-03693-y (2021).
423   33   Abu-Raddad, L. J., Chemaitelly, H., Butt, A. A. & National Study Group for, C.-V. Effectiveness of
424   the BNT162b2 Covid-19 Vaccine against the B.1.1.7 and B.1.351 Variants. *N Engl J Med* **385**, 187-
425   189, doi:10.1056/NEJMc2104974 (2021).
426   34   Thomas, S. J. *et al.* Six Month Safety and Efficacy of the BNT162b2 mRNA COVID-19 Vaccine. *N*
427   *Engl J Med* In press (2021).
428   35   Ku, Z. *et al.* Molecular determinants and mechanism for antibody cocktail preventing SARS-CoV-
429   2 escape. *Nat Commun* **12**, 469, doi:10.1038/s41467-020-20789-7 (2021).
430   36   Cumming, G. The New Statistics: Why and How. *Psychol. Sci.*, 7-29,
431   doi:10.1177/0956797613504966 (2014).
432   37   Andersen, C. Catseyes: Create Catseye Plots Illustrating the Normal Distribution of the Means. R
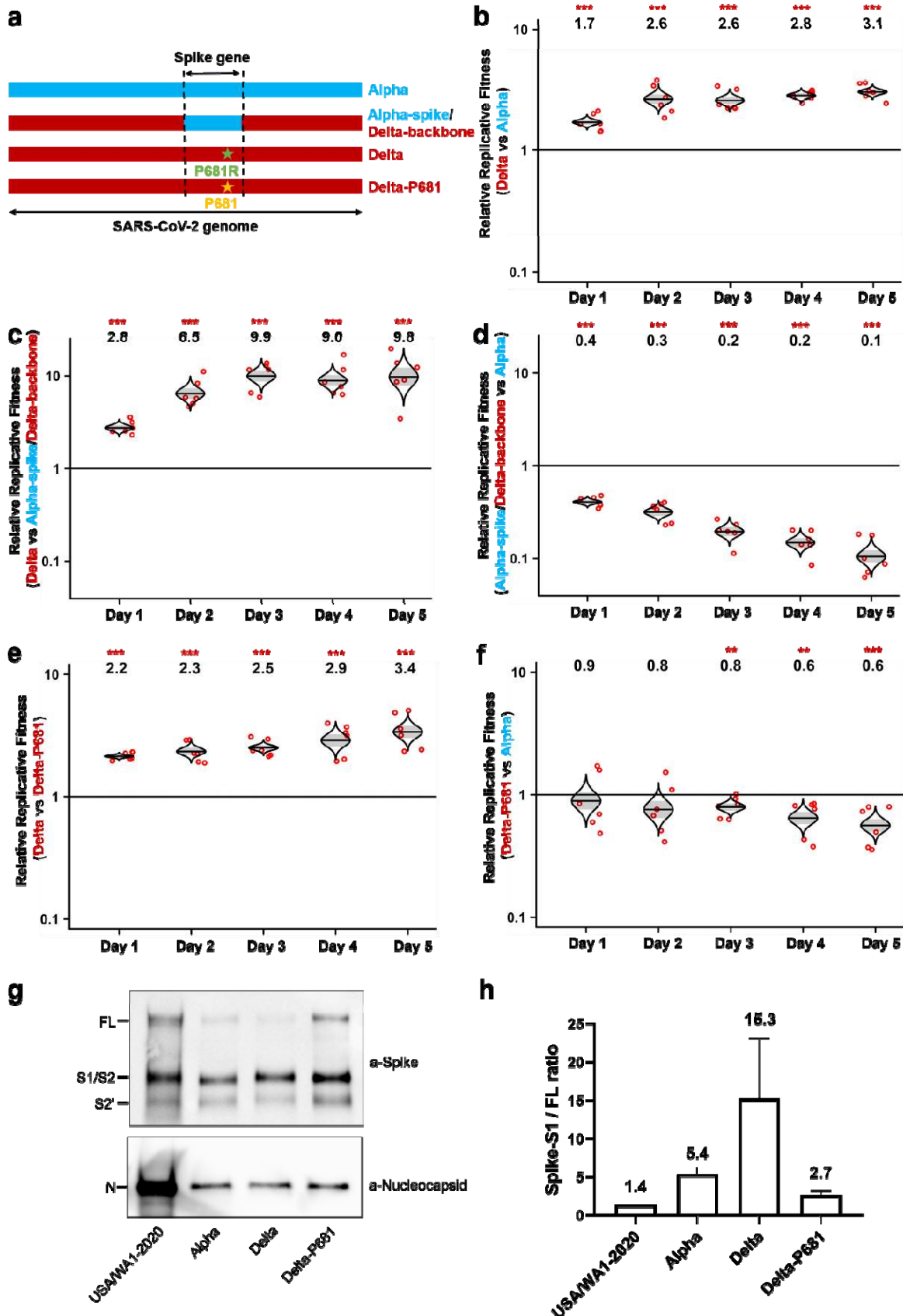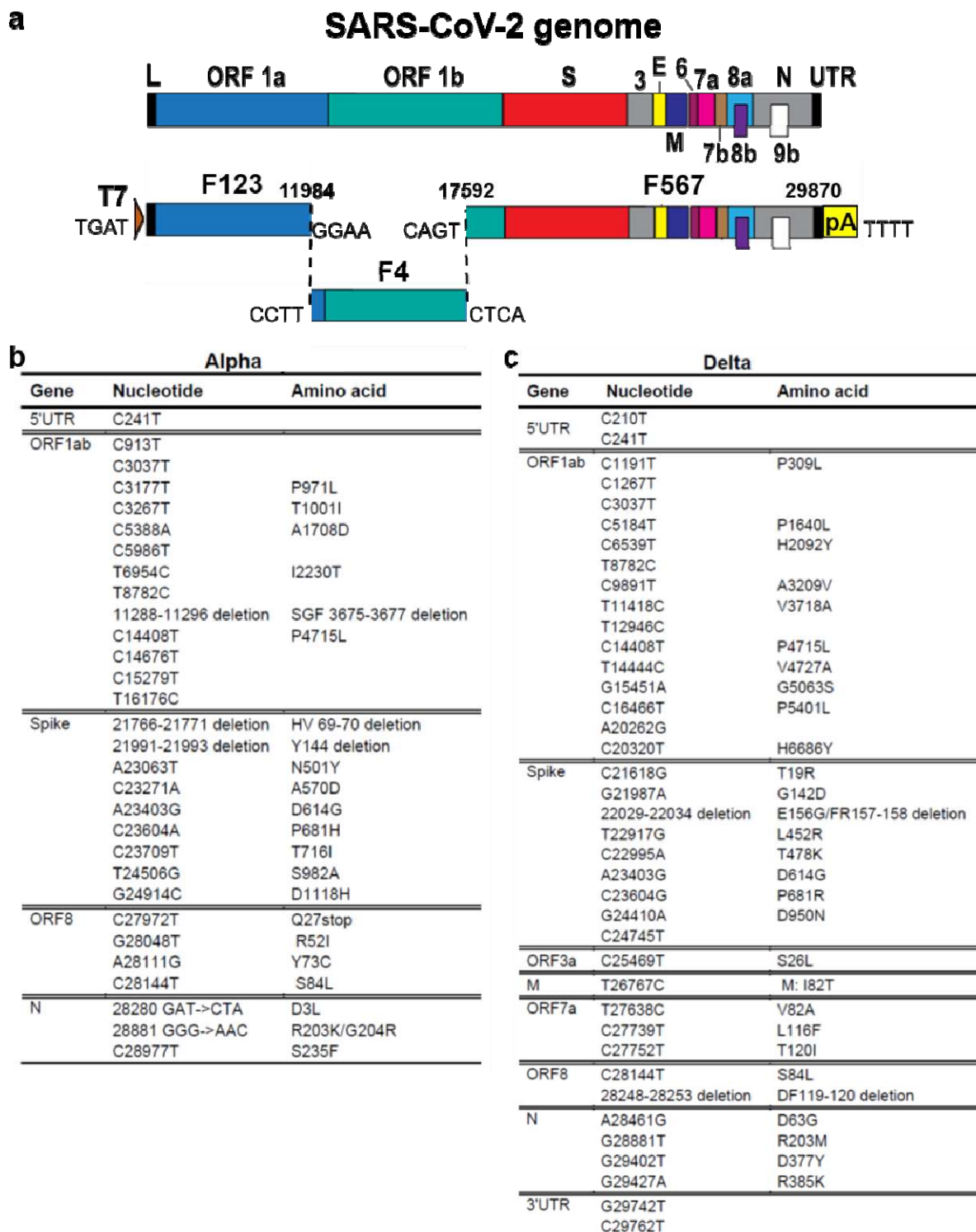433   package version 0.2.3. (2019).

434

435

Figure 1. Delta P681R mutation enhances SARS-CoV-2 fitness over Alpha variant through improving spike protein processing.
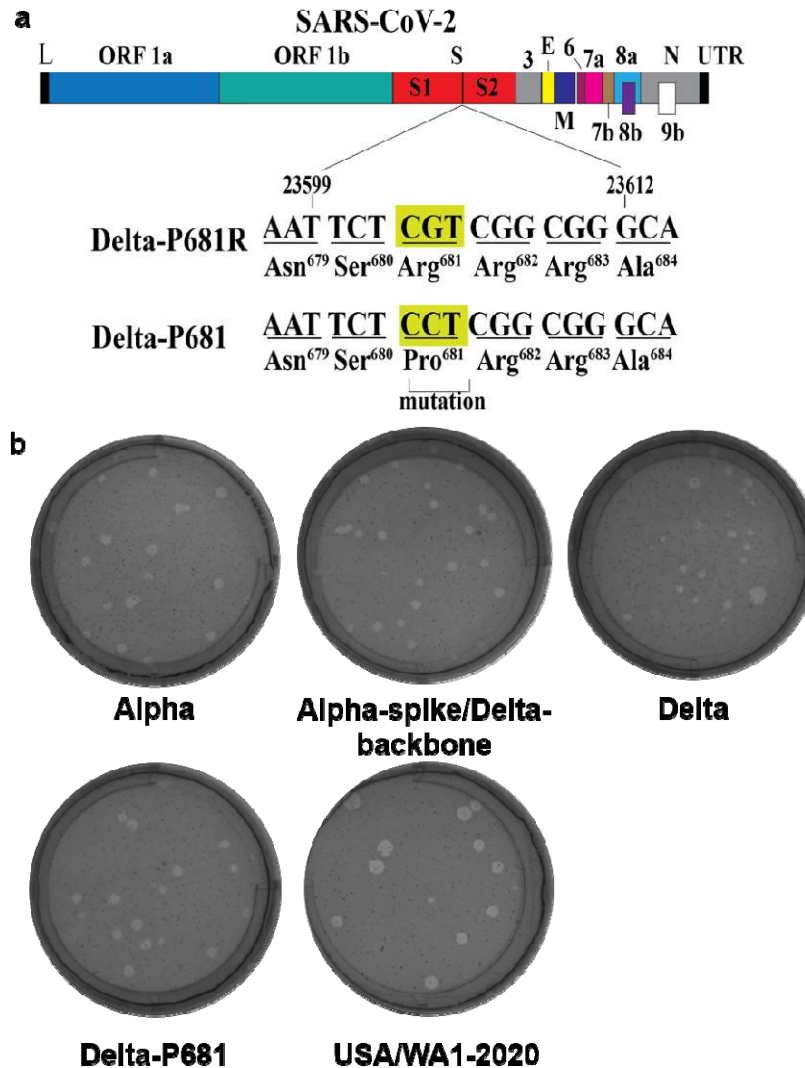
a, Schemes of Alpha variant, Delta variant, Delta variant bearing Alpha-spike, and Delta variant with a P681R-to-P681 reversion. The spike gene of Delta variant was swapped with Alpha variant, resulting in chimeric SARS-CoV-2 "Alpha-spike/Delta-backbone." The Delta P681R mutation was reverted wild-type P681, resulting in "Delta-P681" virus. Blue and red colors indicate Alpha and Delta variants, respectively. **b-f,** Viral replication competitions among Alpha, Delta, Alpha-spike/Delta-backbone, and Delta-P681 viruses on primary human airway epithelial (HAE) cells. Equal PFU of two viruses were mixed and inoculated onto HAE cells at an MOI of 5. Five pairs of viral competition are presented: Delta and Alpha (**b**), Delta and Alpha-spike/Delta-backbone (**c**), Alpha-spike/Delta-backbone and Alpha (**d**), Delta variant and Delta-P618 (**e**), and Delta-P681 and Alpha (**f**). After 2 h incubation, the cells were washed thrice with DPBS and maintained for 5 days. The secreted viruses were collected daily in DPBS after incubation at 37°C for 30 min. Red dots represent individual cell cultures (n=6), the horizontal lines in each catseye represent the mean, shaded regions represent standard error of the mean; y-axes use a $\log_{10}$ scale. Black numbers above each set of values (catseye) indicate the ratios of two viral RNA species. P values are calculated for group coefficient using linear regression model. **$p<0.01$, ***$p<0.001$. **g,** Spike cleavages of purified virions. USA/WA1-2020, Alpha, Delta, and Delta-P681 viruses were purified and analyzed by Western blot using polyclonal antibodies against spike and anti-nucleocapsid antibodies. Full-length spike (FL), cleaved S1/S2, and S2' proteins were annotated. One representative image of two experiments is shown. **h,** Quantification of spike processing of different variants from **g**. Densitometry was performed to quantify the cleavage efficiency of FL spike to S1/S2 subunits using ImageLab 6.0.1. The ratios of S1/S2 over FL were calculated to indicate spike processing efficiencies. The average results of two experiments were presented as mean ± standard deviation.

18

a

b Alpha

Gene	Nucleotide	Amino acid
5'UTR	C241T	
ORF1ab	C913T	
	C3037T	
	C3177T	P971L
	C3267T	T1001I
	C5388A	A1708D
	C5986T	
	T6954C	I2230T
	T8782C	
	11288-11296 deletion	SGF 3675-3677 deletion
	C14408T	P4715L
	C14676T	
	C15279T	
	T16176C	
Spike	21766-21771 deletion	HV 69-70 deletion
	21991-21993 deletion	Y144 deletion
	A23063T	N501Y
	C23271A	A570D
	A23403G	D614G
	C23604A	P681H
	C23709T	T716I
	T24506G	S982A
	G24914C	D1118H
ORF8	C27972T	Q27stop
	G28048T	R52I
	A28111G	Y73C
	C28144T	S84L
N	28280 GAT->CTA	D3L
	28881 GGG->AAC	R203K/G204R
	C28977T	S235F

c Delta

Gene	Nucleotide	Amino acid
5'UTR	C210T	
	C241T	
ORF1ab	C1191T	P309L
	C1267T	
	C3037T	
	C5184T	P1640L
	C6539T	H2092Y
	T8782C	
	C9891T	A3209V
	T11418C	V3718A
	T12946C	
	C14408T	P4715L
	T14444C	V4727A
	G15451A	G5063S
	C16466T	P5401L
	A20262G	
	C20320T	H6686Y
Spike	C21618G	T19R
	G21987A	G142D
	22029-22034 deletion	E156G/FR157-158 deletion
	T22917G	L452R
	C22995A	T478K
	A23403G	D614G
	C23604G	P681R
	G24410A	D950N
	C24745T	
ORF3a	C25469T	S26L
M	T26767C	M: I82T
ORF7a	T27638C	V82A
	C27739T	L116F
	C27752T	T120I
ORF8	C28144T	S84L
	28248-28253 deletion	DF119-120 deletion
N	A28461G	D63G
	G28881T	R203M
	G29402T	D377Y
	G29427A	R385K
3'UTR	G29742T	
	C29762T	

461

Extended Data Figure 1. Construction of infectious cDNA clones for Alpha and Delta variants.
a, Construction of infectious cDNA clones for Alpha and Delta variants. A three-fragment *in vitro* ligation was performed to construct the full-length cDNA clones of Alpha and Delta SARS-CoV-2.
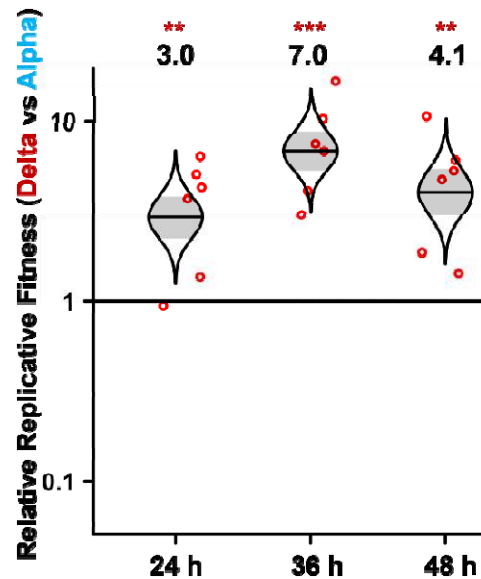
466   The construction method was detailed previously.[12,13] ORFs, the Open reading frames; L, leader
467   sequence; S, spike gene; E, envelope glycoprotein gene; M, membrane glycoprotein gene; N,
468   nucleocapsid gene; UTR, untranslated region. **b,c,** Mutations from Alpha and Delta variants.
469   The whole genome sequences of Alpha (EPI_ISL_999340) (**b**) and Delta (EPI_ISL_2100646) (**c**)
470   were compared to USA/WA1-2020 strain. Nucleotide and amino acid mutations are presented.
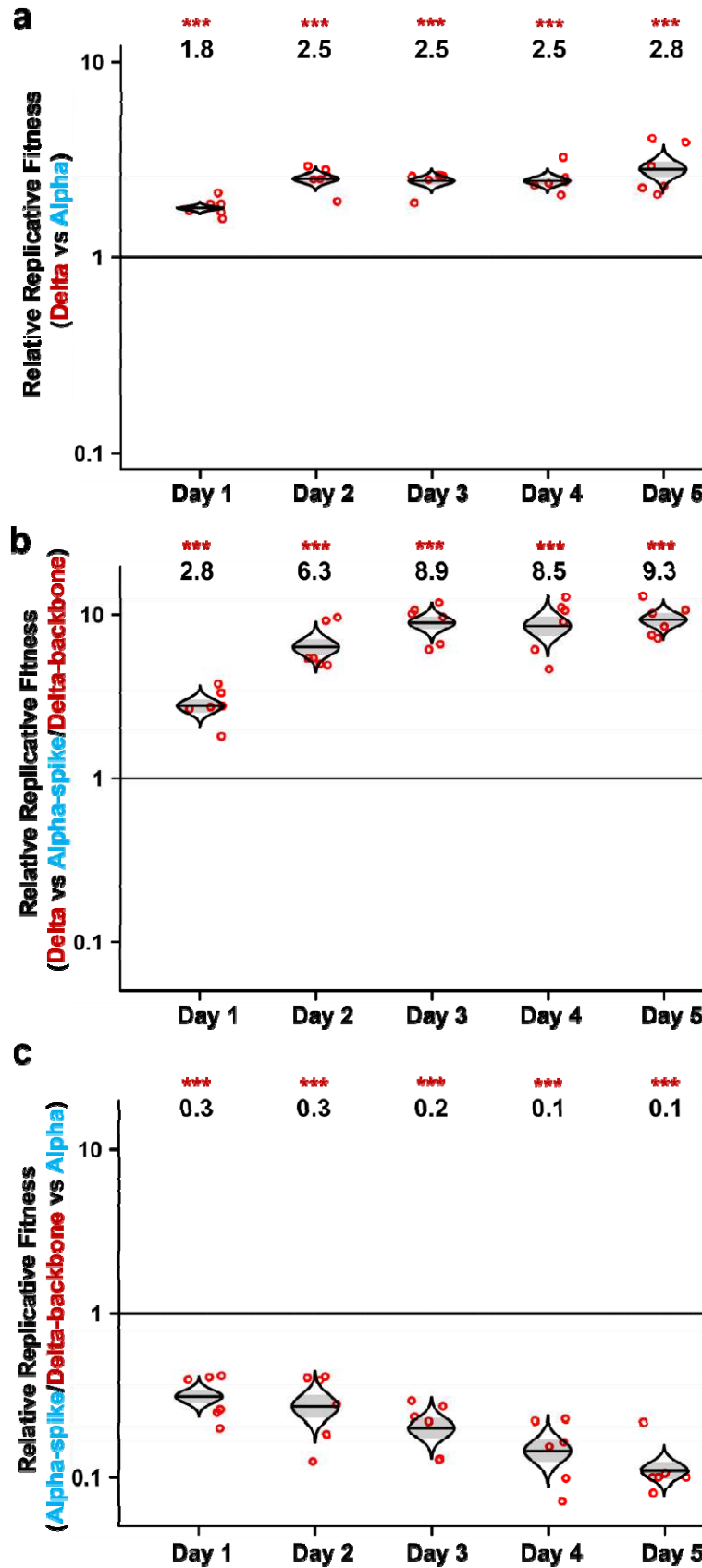471

472

Extended Data Figure 2. Construction of Delta-P681 SARS-CoV-2 and plaque morphologies of different recombinant SARS-CoV-2s.

a, Construction of revertant Delta-P681 SARS-CoV-2. Single nucleotide G-to-C substitution was engineered into the Delta variant to construct Delta-P681 SARS-CoV-2. The nucleotide positions of viral genome are annotated. **b,** Plaque morphologies of Alpha, Alpha-spike/Delta-backbone, Delta, Delta-P681, and USA-WA1/2020 viruses. The plaque images were taken on day 2.5 post infection of Vero E6 cells.
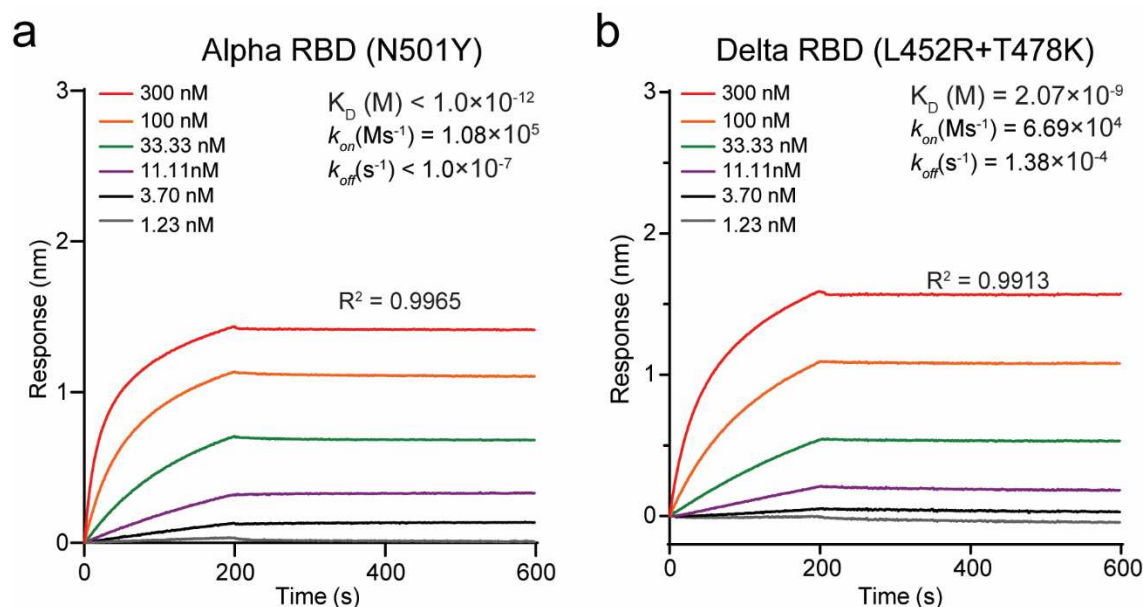
480

Extended Data Figure 3. Viral replication competition between Delta and Alpha variants on Calu-3 cells.
Recombinant Delta and Alpha SARS-CoV-2s were mixed in equal PFUs to infect Calu-3 cells at a total MOI of 0.1. At 2 h post infection, the cells were washed thrice with DPBS to remove free viruses. Culture medium were sampled for Sanger sequencing at 24 h, 36 h, and 48 h post infection. Red dots represent individual cell cultures (n=6); horizontal lines in each catseye represent the mean; shaded regions represent standard error of the mean; y-axes use a $\log_{10}$ scale. Black numbers above each set of values (catseye) indicate the ratios of two viral RNA species. P values are calculated for group coefficient using linear regression model. **$p<0.01$, ***$p<0.001$.

491

Extended Data Figure 4. Validation of viral competition results by next generation sequencing.

a-c, RNA samples from competition assays between Delta and Alpha (**a**), Delta and Alpha-spike/Delta-backbone (**b**), Alpha-spike/Delta-backbone and Alpha (**c**) were initially assessed using Sanger sequencing (**Fig. 1b-d**). The same RNA samples were retested here using next generation sequencing (NGS). Red dots represent individual cell cultures (n=6); the horizontal lines in each catseye represent the mean; shaded regions represent standard error of the mean; y-axes use a $\log_{10}$ scale. Black numbers above each set of values (catseye) indicate the relative fitness estimates. *P* values are calculated for group coefficient using linear regression model. ***$p<0.001$.

Extended Data Figure 5. Binding affinities of Alpha and Delta RBDs to human ACE2 receptor.

a-b, Alpha RBD (**a**) and Delta RBD (**b**) proteins were captured onto protein A biosensors. The biosensors were then dipped into serially diluted human ACE2 protein and buffers to measure the association and dissociation kinetics. The binding affinity-related parameters, including association (K_{on}), dissociation (K_{off}), and affinity (K_D) are shown. The affinity of ACE2 to Alpha RBD (N501Y) is below the detection limit and is presented as $<1.0\times10^{-12}$. The result for Alpha RBD and ACE2 binding was adopted from our previous study[4] for comparison.

512 **Extended Data Table 1. Primer list used for SARS-CoV-2 infectious clones construction,**
513 **RT-PCR and sequencing.**

Construction of Alpha full length and Alpha-backbone infectious clone	Forward primer	Reverse primer
C241T	atctaggtttTgtccgggtgtgaccgaaag	ctttcggtcacacccggacAaaacctagat
C913T	tgcactttgtcTgaacaactggactt	aagtccagttgttcAgacaaagtgca
C3037T	gtattgttctttTtaccctccagatgagg	cctcatctggagggtaAaaagaacaatac
C3177T	ctgctcttcaacTtgaagaagagcaa	ttgctcttcttcaAgttgaagagcag
C3267T	cagacaactaTtattcaaacaattgttgagg	cctcaacaattgtttgaataAtagttgtctg
C5388A	ggctggtgaagctgAtaacttttgtgc	gcacaaaagttaTcagcttcaccagcc
C5986T	attcttatttTacagagcaaccaattg	caattggttgctctgtAaaataagaat
T6954C	gataaatattaCaatttggtttttac	gtaaaaaccaaattGtaatatttatc
11288-11296del	gatactagtttgaagctaaaagactgtgt	acacagtcttttagcttcaaactagtatc
C14408T	tacagtgttcccacTtacaagttttggacc	ggtccaaaacttgtaAgtgggaacactgta
C14676T	gtcaaaccTggtaattttaacaaag	ctttgttaaaattaccAggtttgac
C15279T	gaaaaccctcaTcttatgggttgggat	atcccaacccataagAtgagggttttc
T16176C	ctaatgataacacCtcaaggtattgggga	tcccaataccttgaGgtgttatcattag
C27972T/G28048T	cttaacatcaaccatatgtagttgatgacccgtgtcctattcacttcta	ttatagctcctactctaatataccatttagaatagaagtgaataggaca
A28111G/C28144T	cagtgcatcgatatcggtaattatacagtttcctgtttaccttttac	gtaaaaggtaaacaggaaactgtataattaccgatatcgatgcactg
A28271del/28280-28282GAT-CTA	caaactaaatgtctctaaatggaccccaaaatcagcg	cgctgattttgggggtccatttagagacatttagtttg
28881-28883GGG-AAC	caactccaggcagcagtaaacgaacttctcctgc	gcaggagaagttcgtttactgctgcctggagttg
C28977T	tgagagcaaaatgtttggtaaaggccaaca	tgttggcctttaccaaacattttgctctca
Alpha-F123-F1	cattatacgaagttatattcgatgcggccgctaatacgactcactatagattaaag	gggccgacaacatgaagacagtg
Alpha-F123-F2	acactgtcttcatgttgtcggcccaaatgttaacaaag	ctattacgtttgtaacacatcatacaTgtAgatgaattac
Alpha-F123-F3	gtatgatgtgttacaaacgtaatagagcaacaagag	aggtcgactctagaggatcccacATCGAtggtctcaaaggcttcagtagtatctttagc
Alpha-F4	tgtagaaaacccagatatatt	caaaacactctacacgagcac
Alpha-F567-F1	tatacgaagttatattcgatgcggccgcgtctcagagtgctttggtttatgataataag	cttttgttgtataaacccacaaatg
Alpha-F567-F2	catttgtgggtttatacaacaaaag	caatcaagccagctataaaacc
Alpha-F567-F3	ggttttatagctggcttgattg	cgaggcttcttagaagcctca
Alpha-backbone-F567-F1	tatacgaagttatattcgatgcggccgcgtctcagagtgctttggtttatgataataag	cttttgttgtataaacccacaaatg
Alpha-backbone-F567-F2	catttgtgggtttatacaacaaaag	caatcaagccagctataaaacc
Alpha-backbone-F567-F3	ggttttatagctggcttgattg	cgaggcttcttagaagcctca

26

Construction of Delta full length and Delta-backbone infectious clone	Forward primer	Reverse primer
C210T	GTTTCGTCCGTTTTGCAGCCGATCATC	GATGATCGGCTGCAAAACGGACGAAAC
C241T	ATCTAGGTTTTGTCCGGGTGTGACCGAAAG	CTTTCGGTCACACCCGGACAAAACCTAGAT
C1191T	CCAGTTGCGTCACTAAATGAATGCAACC	GGTTGCATTCATTTAGTGACGCAACTGG
C1267T	GGCAGACGGGTGATTTTGTTAAAGCC	GGCTTTAACAAAATCACCCGTCTGCC
C3037T	GTATTGTTCTTTTTACCCTCCAGATGAGG	CCTCATCTGGAGGGTAAAAAGAACAATAC
C5184T	ACACAACTGATCTTAGTTTTCTGGGTAG	CTACCCAGAAAACTAAGATCAGTTGTGT
C6539T	GAGGTTGGCTACACAGATCTAATGGC	GCCATTAGATCTGTGTAGCCAACCTC
T8782C	ACACATGGTTTAGCCAGCGTGGTGGTAG	CTACCACCACGCTGGCTAAACCATGTGT
C9891T	GATACTTAGTTCTTTATAATAAGTACAAG	CTTGTACTTATTATAAAGAACTAAGTATC
T11418C	CTTGACACTCGCTTATAAAGTTTATTATGG	CCATAATAAACTTTATAAGCGAGTGTCAAG
T12946C	GGTCCTAAAGTGAAGTACTTATACTTTATT	AATAAAGTATAAGTACTTCACTTTAGGACC
C14408T	TACAGTGTTCCCACTTACAAGTTTTGGACC	GGTCCAAAACTTGTAAGTGGGAACACTGTA
T14444C	GTGAGAAAAATATTTGCTGATGGTGTTCCA	TGGAACACCATCAGCAAATATTTTTCTCAC
G15451A	GGTCATGTGTGGCAGTTCACTATATGTT	AACATATAGTGAACTGCCACACATGACC
C16466T	GTAAATCACATAAACTACCCATTAGTTTTCC	GGAAAACTAATGGGTAGTTTATGTGATTTAC
A20262G	GGAAATTGATTTCTTGGAATTAGCTATGG	CCATAGCTAATTCCAAGAAATCAATTTCC
C20320T	GCTATGCCTTCGAATATATCGTTTATGG	CCATAAACGATATATTCGAAGGCATAGC
C21618G	GTGTGTTAATCTTAGAACCAGAACTC	GAGTTCTGGTTCTAAGATTAACACAC
G21987A	GATCCATTTTTGGATGTTTATTACCAC	GTGGTAATAAACATCCAAAAATGGATC
22029-22034 deletion	GAAAGTGGAGTTTATTCTAGTGCGAATAATTGC	ATAAACTCCACTTTCCATCCAACTTTTGTTGTT
T22917G	GGTGGTAATTATAATTACCGGTATAGATTGTTTAGG	CCTAAACAATCTATACCGGTAATTATAATTACCACC
C22995A	GGCCGGTAGCAAACCTTGTAATGGTG	CACCATTACAAGGTTTGCTACCGGCC
A23604G	GACTAATTCTCGTCGGCGGGCACGTAGTGT	ACACTACGTGCCCGCCGACGAGAATTAGTC
G24410A	GGAAAACTTCAAAATGTGGTCAACC	GGTTGACCACATTTTGAAGTTTTCC
C24745T	CTCATGGTGTAGTTTTCTTGCATGTGAC	GTCACATGCAAGAAAACTACACCATGAG
C25469T	GATGCTACTCCTTTAGATTTTGTTCGCG	CGCGAACAAAATCTAAAGGAGTAGCATC
T26767C	CCGGTGGAATTGCTACCGCAATGGCTTG	CAAGCCATTGCGGTAGCAATTCCACCGG
T27638C	CGTGCCAGATCAGCTTCACCTAAACTGT	ACAGTTTAGGTGAAGCTGATCTGGCACG
C27739T/C27752T	TCAAAAGAAAGATAGAATGATTGAACTTTCA	CATTCTATCTTTCTTTTGAATGTGAAGCAAAGTG
C28144T	TCGGTAATTATACAGTTTCCTGTTTACCTTTTAC	GTAAAAGGTAAACAGGAAACTGTATAATTACCGA

28248-28253 deletion	GACGTTCGTGTTGTTTTAATCTAAACGAACAAACT	AGTTTGTTCGTTTAGATTAAAACAACACGAACGTC
28271 deletion	GAACAAACTAAATGTCTGATAATGGACCCC	GGGGTCCATTATCAGACATTTAGTTTGTTC
A28461G	CATGGCAAGGAAGGCCTTAAATTCCCTC	GAGGGAATTTAAGGCCTTCCTTGCCATG
G28881T	TCCAGGCAGCAGTATGGGAACTTCTCCTGC	GCAGGAGAAGTTCCCATACTGCTGCCTGGA
G29402T/G29427A	GCTTATGAAACTCAAGCCTTACCGCAGAAACAGAAGAAAC	GTTTCTGCGGTAAGGCTTGAGTTTCATAAGCCTTCTTCTT
G29742T/C29762T	CACTCGGAGTACGATCGAGTGTATAGTGAACAAT	ACTATACACTCGATCGTACTCCGAGTGGCCTCGG
Delta-F123-F1	cattatacgaagttatattcgatgcggccgctaatacgactcactatagattaaag	gggccgacaacatgaagacagtg
Delta-F123-F2	acactgtcttcatgttgtcggcccaaatgttaacaaag	aggtcgactctagaggatcccacATCGAtggtctcaaaggcttcagtagtatctttagc
Delta-F4	cctcttacaacagcagccaaact	caaaacactctacacgagcac
Delta-F567	tatacgaagttatattcgatgcggccgcgtctcagagtgcttggtttatgataataag	caaacatgagaattggtcgacggccc
Delta-backbone-F567-F1	tatacgaagttatattcgatgcggccgcgtctcagagtgcttggtttatgataataag	cttttgttgtataaacccacaaatg
Delta-backbone-F567-F2	catttgtgggtttatacaacaaaag	caatcaagccagctataaaacc
Delta-backbone-F567-F3	ggttttatagctggcttgattg	cgaggcttcttagaagcctca
RT-PCR for Sanger sequencing	**Forward primer**	**Reverse primer**
Delta vs Delta-P681	tccacttttaagtgttatggag	gttaaagcacggtttaattgtg
Delta-P681 vs Alpha	tccacttttaagtgttatggag	gttaaagcacggtttaattgtg
Delta vs Alpha	tccacttttaagtgttatggag	gttaaagcacggtttaattgtg
Alpha-spike/Delta-backbone vs Alpha	tgtagaaaacccagatatatt	tggaaaaccagctgatttgtc
Delta vs Alpha-spike/Delta-backbone	tccacttttaagtgttatggag	gttaaagcacggtttaattgtg
RT-PCR for NGS	**Forward primer**	**Reverse primer**
Delta vs Alpha	ggttttaattgttactttcctttaca	aagaacacctgtgcctgtt
Alpha-spike/Delta-backbone vs Alpha	acagtgttcccacctacaagt	ccagaagcagcgtgcatagc
Delta vs Alpha-spike/Delta-backbone	ggttttaattgttactttcctttaca	aagaacacctgtgcctgtt
Sanger sequencing	**Forward primer**	
Delta vs Delta-P681	aggatgttaactgcacaga	
Delta-P681 vs Alpha	aggatgttaactgcacaga	
Delta vs Alpha	gattgctgattataattata	
Alpha-spike/Delta-backbone vs Alpha	gttgacactgacttaacaaagcc	
Delta vs Alpha-spike/Delta-backbone	gattgctgattataattata	

514

515

516 **Extended Data Table 2. The input and output viral RNA ratios in competition assays**
517 **detected by sanger sequencing.**

Groups	HAE			Calu-3		
	Days	Input ratio	Output ratio	Hours	Input ratio	Output ratio
Delta vs Alpha	Day 1	1.24	2.10	24h	1.53	4.56
	Day 2	1.24	3.24	36h	1.53	10.65
	Day 3	1.24	3.17	48h	1.53	6.21
	Day 4	1.24	3.51			
	Day 5	1.24	3.78			
Delta vs Alpha-spike/Delta-backbone	Day 1	1.07	2.97			
	Day 2	1.07	6.93			
	Day 3	1.07	10.60			
	Day 4	1.07	9.64			
	Day 5	1.07	10.53			
Alpha-spike/Delta-backbone vs Alpha	Day 1	1.45	0.59			
	Day 2	1.45	0.46			
	Day 3	1.45	0.28			
	Day 4	1.45	0.22			
	Day 5	1.45	0.15			
Delta vs Delta-P681	Day 1	0.95	2.05			
	Day 2	0.95	2.20			
	Day 3	0.95	2.38			
	Day 4	0.95	2.77			
	Day 5	0.95	3.25			
Delta-P681 vs Alpha	Day 1	1.51	1.33			
	Day 2	1.51	1.13			
	Day 3	1.51	1.21			
	Day 4	1.51	0.97			
	Day 5	1.51	0.85			

518